High-Frequency Sound Propagation near Magnetic Phase Transitions*

T. J. Moran and B. Lüthi
Department of Physics, Rutgers University, New Brunswick, New Jersey 08903
(Received 1 March 1971)

The results of ultrasonic attenuation and velocity experiments near the magnetic phase transitions in $RbMnF_3$ and MnF_2 are presented. For $T > T_N$, the data give additional evidence that the sound couples to the spin-energy-density fluctuations which decay via spin-lattice relaxation. The attenuation results for $RbMnF_3$ could be fitted with a single relaxation formula for the frequency range 90–930 MHz and for the temperature range of $\epsilon\,[=(T-T_N)/T_N]$ from 10^{-4} to 10^{-2}. The spin-lattice relaxation time τ_L was found to vary from 4×10^{-10} to 2×10^{-10} sec in the same ϵ range. Furthermore, both the critical attenuation and velocity changes are independent of sound-wave propagation direction. In MnF_2, we found from the critical velocity dispersion a constant relaxation time $\tau_L = (2.7\pm0.2)\times10^{-9}$ sec for $\epsilon \geq 10^{-3}$, in good agreement with Kawasaki and Ikushima's quoted value. A small divergence was found for smaller ϵ. For $T < T_N$, it was found that the maxima of the attenuation and the minima of the velocity shifted to lower temperatures with increasing frequency in $RbMnF_3$. In addition, in $RbMnF_3$, a second attenuation peak was found below T_N which shifted to lower temperatures with increasing frequency. This subsidiary attenuation peak was found to be strongly sample dependent. In MnF_2, broad attenuation maxima and velocity minima are observed in the ordered region. Possible mechanisms for these effects are discussed.

I. INTRODUCTION

Sound propagation near second-order magnetic phase transitions has been the subject of many experimental and theoretical investigations in recent years.[1] From ultrasonic attenuation experiments in the paramagnetic phase the materials studied can be classified into two groups: magnetic metals and magnetic insulators. In magnetic metals (such as the rare-earth metals Gd, Tb, Dy, and Ho and the transition metal Ni), strong anomalies in the attenuation coefficient α were observed, with α of the form

$$\alpha = B\omega^2\epsilon^{-\eta}, \tag{1}$$

where $\omega = 2\pi\nu$, ν is the sound-wave frequency, ϵ is the reduced temperature $(T-T_N)/T_N$, and η, the critical exponent, varies between 1.0 and 1.6. In the case of typical insulators, such as EuO, MnF_2, and $RbMnF_3$, rather small exponents η are observed, ranging from 0 (EuO) to ~0.25 ($RbMnF_3$).

This different behavior could be explained by the assumption that in magnetic metals, with long-range exchange interactions, the sound wave couples predominantly to order-parameter fluctuations, whereas in magnetic insulators, with essentially only nearest-neighbor exchange interactions, the sound wave couples predominantly to the spin energy density.

Mode-mode coupling theories[2,3] give an attenuation expression of the form $\alpha \propto \omega^2 C\tau_c$ ($\omega\tau_c \ll 1$), where C is the magnetic specific heat and τ_c is the characteristic critical spin-fluctuation relaxation time. The comparison with Eq. (1) is quite satisfactory with regard to the exponent η and it also gives the correct order of magnitude of the effect [the constant B in Eq. (1)] for the case of magnetic metals.

In magnetic insulators it was assumed that the spin-energy-density fluctuations decay either by energy diffusion[4] or by spin-lattice relaxation.[5] The latter process gives an attenuation coefficient[5] $\alpha \propto \omega^2 C^2$ for $\omega\tau_L \ll 1$, where $\tau_L (= C/\gamma)$ is the spin-lattice relaxation time, and γ is a constant which does not diverge at T_N. Recently, Huber[6] was able to calculate τ_L for the magnetic insulators mentioned and found substantial agreement with the τ_L determined experimentally in $RbMnF_3$[7] and MnF_2.[8] Therefore, it seems that the low-frequency behavior of ultrasonic attenuation in the paramagnetic phase is quite well understood.

Recent high-frequency ultrasonic experiments revealed interesting features in the ordered phase.[9] Large shifts of the attenuation peaks to lower temperatures with increasing frequency were found, indicating that new mechanisms of sound-wave damping come into play in the ordered region.

In this paper we present new measurements of attenuation and velocity in $RbMnF_3$ and MnF_2 in the frequency range 30–930 MHz in the disordered and ordered regions. This wide frequency range enables us to study sound propagation from $\omega\tau \ll 1$ to $\omega\tau > 1$. In the paramagnetic phase the sound propagation effects can be quantitatively accounted for in the whole frequency region, using single relaxation-time mechanisms as indicated above. For $T \lesssim T_N$, we also observe shifts in the attenuation and velocity peaks as well as additional attenuation peaks at lower temperatures, and possible mechanisms for these phenomena are suggested.

In Sec. II, we list the formulas necessary for the quantitative comparison of experiment and theory for the paramagnetic region. Then we give experimental details, and details about the samples and the method used in the evaluation of the data. Finally, we show results and discuss them.

II. THEORY

In this section we list the formulas necessary for a quantitative comparison with our experiments for the paramagnetic region.

The dominant spin-phonon coupling mechanism responsible for the critical effects is the strain modulation of the exchange interaction[1]:

$$H' = A \sum_{i,R} \left(\frac{\partial J}{\partial \vec{R}} \cdot \vec{e}_q \right) (\vec{R} \cdot \vec{q}) e^{i(\vec{q} \cdot \vec{R}_i)} (\vec{S}_i \cdot \vec{S}_{i+R}), \quad (2)$$

where $J(\vec{R})$ is the exchange constant, $\vec{q}$ is the wave vector, $\vec{e}_q$ is the sound-wave polarization vector, A is the sound-wave amplitude, and $\vec{S}_i$ is the spin at site i.

As outlined in the Introduction and as shown in greater detail below, our sound-propagation experiments in the paramagnetic region in $RbMnF_3$ and MnF_2 can be explained with a sound-wave–spin-energy-density coupling, where the spin-energy-density fluctuations decay predominantly via a single spin-lattice relaxation time. Attenuation and velocity dispersion expressions, valid for the whole $\omega\tau$ range, applied to this case, have been derived previously[10]:

$$\alpha(\omega) \propto \mathrm{Re} \frac{\omega^2 C}{i\omega + 1/\tau} = \frac{\omega^2 C \tau}{1 + \omega^2 \tau^2} , \quad (3a)$$

$$\frac{v(\omega) - v(0)}{v(0)} \propto - \frac{v(0)}{2\omega} \mathrm{Im} \frac{\omega^2 C}{i\omega + 1/\tau} = \tfrac{1}{2} v(0) C \frac{\omega^2 \tau^2}{1 + \omega^2 \tau^2} . \quad (3b)$$

Here Re and Im denote real and imaginary parts, respectively. The zero-frequency velocity change $\Delta v(0)$ has the form[1,8,11,12]

$$\Delta v(0)/v_\infty \propto - \omega^0 C . \quad (4)$$

Here v_∞ is the normal noncritical velocity. Equation (4) has been discussed in detail before.[1] In the limit $\omega\tau \ll 1$, one can determine the relaxation time τ from a combination of α and $\Delta v(0)/v_\infty$[1,8,11]:

$$\frac{1}{\tau} = - \frac{\omega^2}{v_\infty} \frac{\Delta v(0)/v_\infty}{\alpha} . \quad (5)$$

In the ordered region various different physical mechanisms can affect the sound propagation; these will be discussed in Sec. IV D. No theory of sound attenuation has been developed so far for the ordered region near the phase transition.

III. EXPERIMENT

We investigated three $RbMnF_3$ single crystals (labeled as I, II, and III), and one MnF_2 crystal. Crystal I was grown at IBM, the others purchased from Semi-Elements. Crystals II and III had some small visible air bubbles in them, and the others looked perfect. All the crystals had parallel end faces polished within optical accuracy. The crystallographic orientations as indicated on the graphs in Sec. IV were within 0.5°, except for $RbMnF_3$ II [111] which is 4° off the [111] direction. Some data on crystals I, II, and MnF_2 were given previously.[1,7]

The velocity measurements were carried out using a phase-comparison method[13] capable of resolving velocity changes of 1 part in 10^7 with a good echo pattern. For the attenuation measurements we used a calibrated attenuator and a boxcar integrator (model PAR160) as a peak detector. Except for the highest frequencies (> 400 MHz in $RbMnF_3$ and > 90 MHz in MnF_2), we always measured more than one echo. Resonant X-cut quartz transducers (10- or 30-MHz fundamental) were used.

The sample was embedded in a copper block with a resistance thermometer attached directly to the sample. This assembly was then enclosed in a vacuum jacket, the lower section of which was a hollow copper block with a heater wound around the outside. A thermocouple was attached to this block and for measurements above 77 °K the systems were isolated from the liquid-nitrogen bath by a second vacuum jacket. The temperature was controlled by a feedback network with the thermocouple. Below 77 °K the second vacuum jacket was removed and the temperature of the nitrogen bath was controlled by pumping.

A calibrated platinum resistance thermometer with a resolution of 0.25 mdeg and absolute accuracy of 20 mdeg was used to measure the sample temperature for all measurements except some attenuation measurements in $RbMnF_3$ II. A germanium resistance thermometer was used for these measurements. Thermal gradients were measured with a differential thermocouple and were less than the 10-mdeg resolution of the thermocouple.

Figure 1 shows a typical attenuation and velocity result for $RbMnF_3$ I [111] in the temperature range 58–270 °K. In the case of the attenuation for $T > T_N$, one notices that the measured attenuation flattens above $T \sim 110$ °K and is approximately constant for $T > 170$ °K. Therefore the background choice in this case presents little problem and is taken as the constant value above 170 °K. It should be pointed out, however, that different "reasonable" choices of the background attenuation have little effect on the critical attenuation since the main contribution to this critical attenuation only comes from a region within a few degrees of T_N. We will discuss the

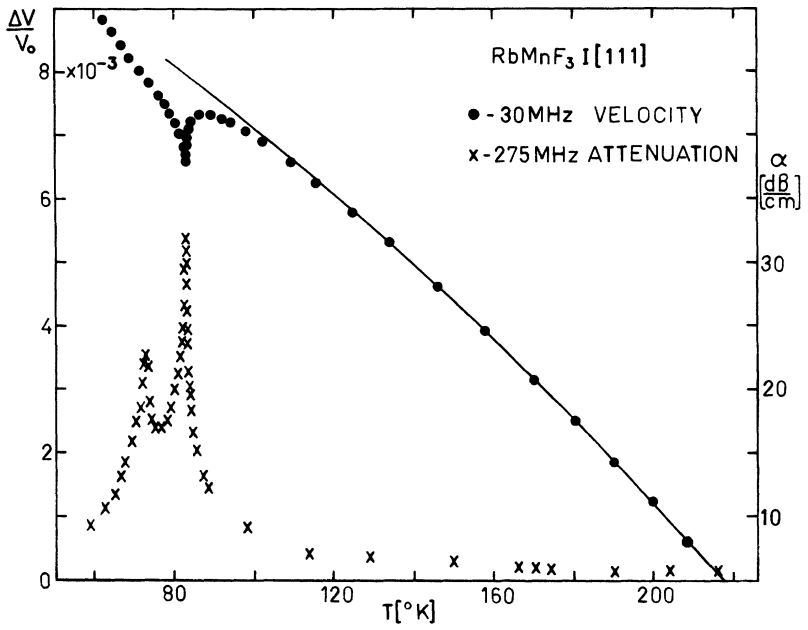

FIG. 1. Velocity and attenuation changes in $RbMnF_3I$ [111] as a function of temperature. Full line is estimated background in the paramagnetic region (see text).

second attenuation peak in the ordered region in Sec. IV D.

The same is true for the critical velocity changes. A linear background choice near T_N usually gives a fair approximation of the critical velocity change.[1] However, in this paper we are not only interested in the temperature dependence of the velocity change, but also in its absolute magnitude, in order to get the most reliable value for the relevant relaxation time τ using Eq. (5). Therefore, we employed a procedure first used by Leisure and Moss[14] to get the best background velocity correction. We approximated the velocity change by a polynomial over a temperature region of ~ 100 °K and extrapolated this function into the critical region. The actual form of this polynomial was

$$\Delta v/v_a = 113.74\times10^{-4}(1 - 3.10^{-3}T - 7.32\times10^{-6}T^2),$$

where v_a is the velocity at 220 °K, and T is in °K. It is shown by the solid line in Fig. 1. No thermal-expansion corrections were applied for $RbMnF_3$ since they are negligible.[15] Unlike the attenuation at higher frequencies, no additional effects are seen in the 30-MHz velocity curve in the ordered region. This will be discussed in Sec. IV D.

IV. RESULTS AND DISCUSSION

First, we present velocity and attenuation results for the paramagnetic region and then we discuss the effects in the ordered region.

A. $RbMnF_3$ Velocity Measurements for $T > T_N$

Velocity measurements in this material in the vicinity of the Néel temperature T_N have been given before.[1,16,17] It was shown in Ref. 1 that there was no frequency dependence, within the accuracy of the experiment, up to 70 MHz in accord with Eq. (4). Here we would like to show more results with increased sensitivity up to 150 MHz, where some frequency dependence of the critical sound velocity change is clearly noticeable. One expects such dispersion, according to Eq. (3b) as soon as the condition $\omega\tau \ll 1$ is no longer fulfilled.

In Fig. 2, we show a linear plot of the velocity change $\Delta v/v$ vs temperature for $RbMnF_3I$ [111], the crystal we investigated previously,[1] and whose over-all velocity change was shown in Fig. 1. Whereas in the background region ($T > 150$ °K) the velocity changes for the different frequencies coincided within 1 part in 10^5, one notices differences in the vicinity of T_N as large as 0.88×10^{-4} from 30 to 90 MHz and 2.4×10^{-4} from 30 to 150 MHz. These changes are even more clearly seen in Fig. 3, where we plot the critical change of the sound velocity vs reduced temperature ϵ for the various frequencies. The necessary background correction was applied in the manner discussed in Sec. III. The determination of T_N will be explained later on in Sec. IV D. One notices in Fig. 3 a logarithmic dependence for two decades in reduced temperature ϵ for 30 MHz, similar to the results in Ref. 1 and in agreement with Eq. (4). There is a noticeable flattening of the velocity change for $\epsilon < 10^{-4}$. This was noticed before in the attenuation measurements[7] and is attributed to a smearing out of the transition due to imperfections. For 90 MHz, a small suppression of these critical velocity changes

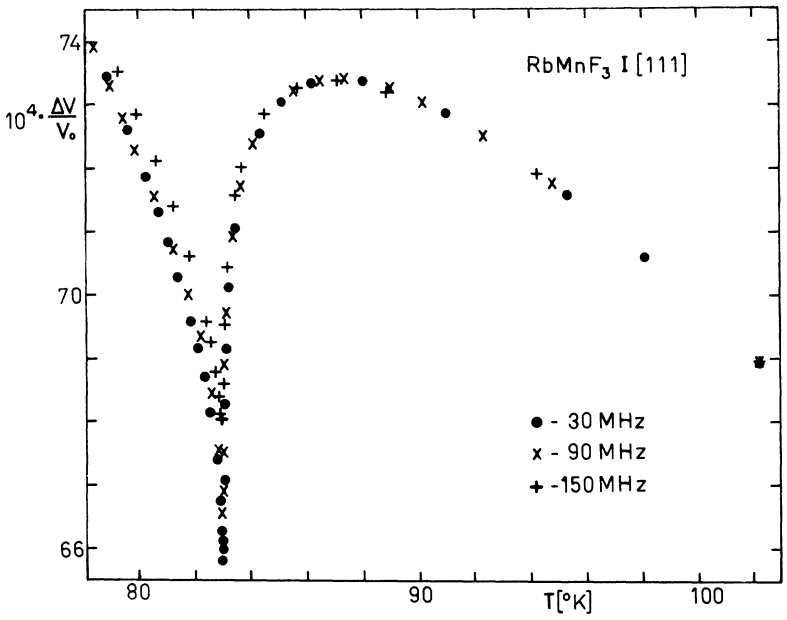

FIG. 2. Linear plot of velocity changes vs temperature for various frequencies in $RbMnF_3$I [111].

is already noticeable for $\epsilon \leqslant 10^{-3}$ and is even more enhanced for 150 MHz (Fig. 3). This is in agreement with Eq. (3b), which predicts a suppression of critical velocity changes. We did not attempt to make a quantitative comparison because we could not cover a large enough range of $\omega\tau$ in the case of $RbMnF_3$. The $\omega\tau \sim 1$ occurs, as discussed below, for $\nu = 450$ MHz at $\epsilon = 3.6 \times 10^{-4}$. Such a comparison will be done later, however, for the case of MnF_2 because there the $\omega\tau \sim 1$ condition is already met for $\nu \sim 60$ MHz.[8]

Measurements in $RbMnF_3$ II for two different propagation directions [100] and [111], respectively, indicate an isotropic critical velocity change, i.e.,

$$\left(\frac{\Delta v\,(T)}{v}\right)_{111} \Big/ \left(\frac{\Delta v\,(T)}{v}\right)_{100} = 0.9 \pm 0.2.$$

This was already noted before,[1] using data from different laboratories. A spin-phonon coupling such as that given by Eq. (2) leads to isotropic critical velocity changes for cubic materials,[8] in accord with our experimental findings.

B. Attenuation Measurements for $RbMnF_3$ for $T > T_N$

The low-frequency ultrasonic attenuation results for $RbMnF_3$, with a critical exponent η of ~ 0.25, have been a puzzle for a long time. Following Kawasaki's suggestion[5] that a sound-wave coupling

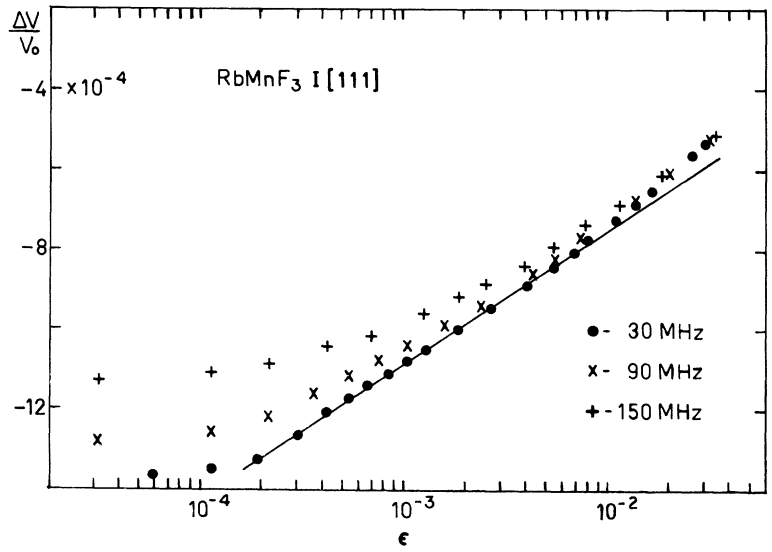

FIG. 3. Semilogrithmic plot of fractional critical velocity changes vs reduced temperature ϵ in $RbMnF_3$I [111].

to the spin energy density of the system, involving a spin-lattice relaxation, may account for these results, the predicted C^2 dependence of the critical attenuation was observed for low frequencies[7] ($\nu < 250$ MHz). Subsequently, Huber[6] calculated the spin-lattice relaxation times for various magnetic insulators for $T > T_N$ and found substantial agreement with the values determined experimentally using Eq. (5). There is a twofold reason for the rather fast spin-lattice relaxation time in $RbMnF_3$ ($\tau_L \sim 2\times10^{-10}$ sec).[6] First, in contrast to the spin-lattice relaxation of dilute paramagnetic ions in salts, where only strain modulation of the crystal field is an efficient mechanism for S-state ion relaxation, in concentrated salts the spin-phonon coupling of Eq. (2), which is responsible for all the critical sound-wave propagation effects, is also responsible for the spin-lattice relaxation. Second, the energy of the lowest acoustic-phonon branch amounts to ~104 °K at the Brillouin zone. Therefore, essentially all the phonons of the acoustic branch can help in the spin-lattice relaxation for $T \gtrsim 83$ °K, giving a large enhancement factor.

One expects the attenuation to be governed by Eq. (3a), which is valid for a single relaxation time if the spin-lattice relaxation mechanism is the only one of importance. That this indeed applies for $RbMnF_3$ is shown in Figs. 4 and 5, where we have plotted the critical attenuation vs the function $\omega^2\tau^2/(1+\omega^2\tau^2)$. This form of the function follows from Eq. (3a) for $\tau = \tau_L = C/\gamma$. The τ was determined experimentally from the low-frequency critical attenuation and velocity changes according to Eq. (5). The values of τ determined from the [100] and [111] samples agreed within a factor of 2. However, both Figs. 4 and 5 are plotted against the τ determined from the [100] sample, which gave the better fit. The T_N determination is explained in Sec. IV D. One sees from Figs. 4 and 5 that the critical attenuation is very well described by the single relaxation formula. Notice that for this fit in Fig. 4 frequencies in the range 90–930 MHz were used and in Fig. 5 from 90 to 630 MHz. The temperature range used was $10^{-4} \lesssim \epsilon \lesssim 10^{-2}$, which comprised the power-law region for smaller frequencies.[7] The range in $\omega\tau$ covered is $\sim 0.01 \lesssim \omega\tau \lesssim 3$ in Fig. 4.

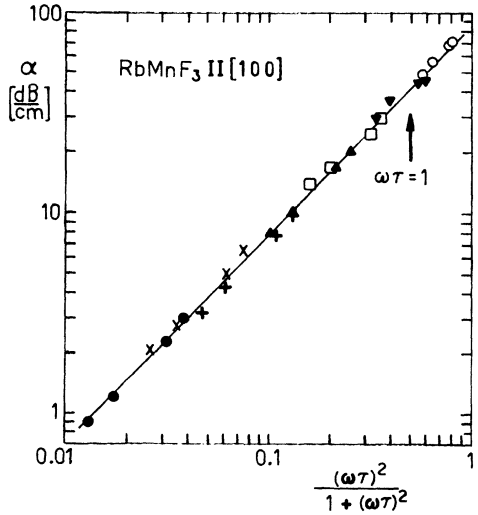

FIG. 4. Critical attenuation vs $(\omega\tau)^2/[1+(\omega\tau)^2]$ for various temperatures and frequencies: ●, 90 MHz; ×, 133 MHz, +, 180 MHz; ▲, 270 MHz; □, 349 MHz; ▼, 570 MHz; ○, 930 MHz. The sample is $RbMnF_3$ II [100].

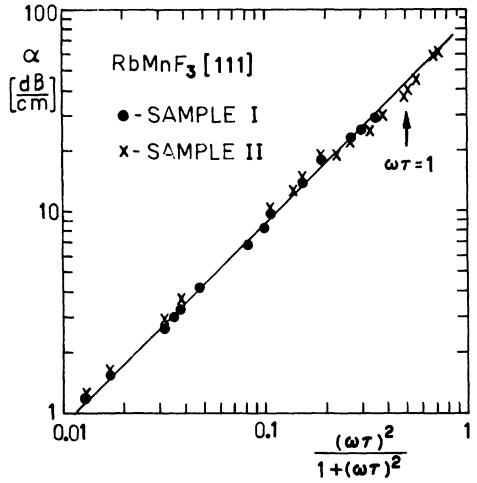

FIG. 5. Critical attenuation vs $(\omega\tau)^2/[1+(\omega\tau)^2]$ for various temperatures and frequencies. The samples are $RbMnF_3$ I [111] and $RbMnF_3$ II [111]. The frequencies range from 90 to 630 MHz.

The experimental spin-lattice relaxation time varied between $2\times10^{-10} < \tau_L < 4\times10^{-10}$ sec for $1.2\times10^{-2} > \epsilon > 4\times10^{-4}$. It is interesting to compare τ_L with the critical relaxation time τ_c for spin fluctuations in $RbMnF_3$ as determined by inelastic neutron scattering.[18] According to the dynamical scaling laws the temperature variation of τ_c is much stronger. For the same temperature region $1.7\times10^{-2} > \epsilon > 4\times10^{-4}$, τ_c varies as $0.08\times10^{-10} < \tau_c < 3\times10^{-10}$, i.e., $\tau_c \ll \tau_L$ over most of the temperature region.

Comparing Figs. 4 and 5 one can deduce $\alpha(T)_{111}/\alpha(T)_{100} = 1.15 \pm 0.15$, i.e., the critical attenuation is isotropic with regard to propagation directions. This is at variance with the result quoted in Ref. 1, where this ratio was deduced from experiments done at different laboratories. This latter result should therefore be discarded. One expects such an isotropic behavior because of the isotropic critical velocity changes quoted above and in Eq. (5), in which the spin-lattice relaxation time τ_L is an isotropic quantity.

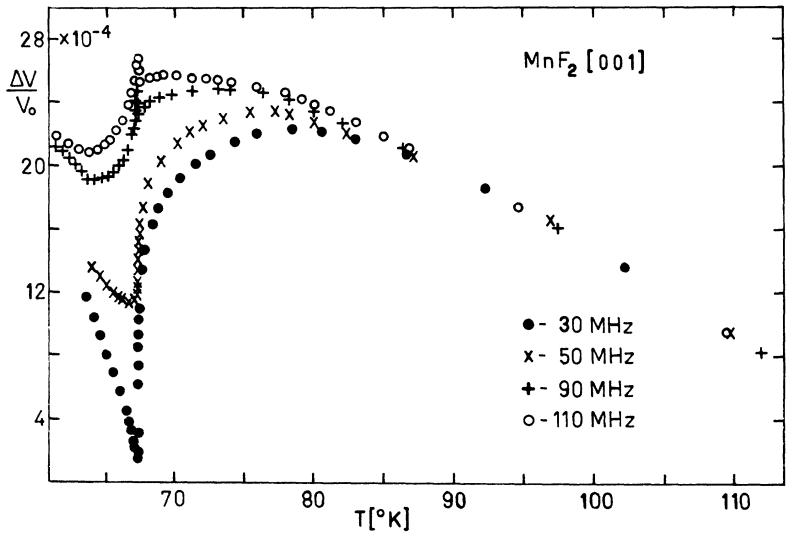

FIG. 6. Sound velocity changes in MnF_2 for [001] propagation.

C. Sound Propagation in MnF_2 for $T > T_N$

Sound propagation in MnF_2 has been studied extensively.[1,8,9,14] Here we would like to show some velocity measurements which clearly show the effect of dispersion. Attenuation results will be given in Sec. IV D. The relevant relaxation time in this case was deduced to be $\tau \sim 3\times10^{-9}$ sec.[8] The difference in τ_L between MnF_2 and $RbMnF_3$ arises from the different zone-boundary phonon energies which are about 140 °K for MnF_2.[6] Therefore for $T \sim 68$ °K, only part of the acoustic-phonon branch can contribute to the spin-lattice relaxation; consequently τ_L for MnF_2 is larger than for $RbMnF_3$. Thus $\omega\tau \sim 1$ at $\nu \sim 60$ MHz.

Figure 6 shows velocity changes in MnF_2 for c-axis propagation and for a frequency range 30–110 MHz. Whereas for smaller frequencies one still

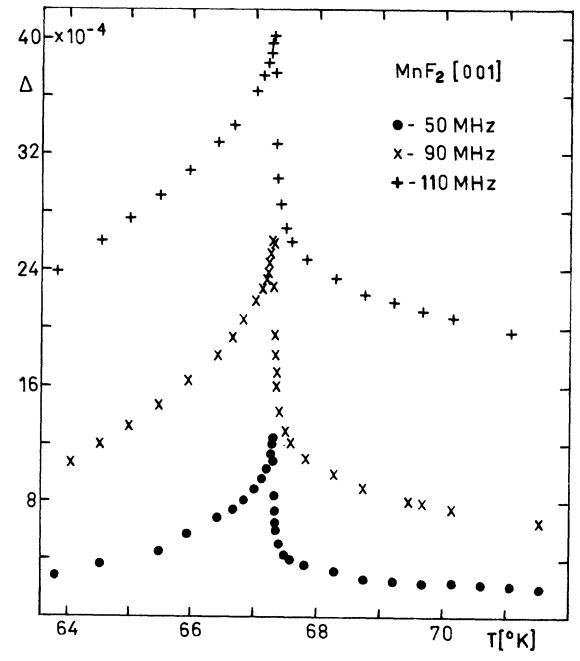

FIG. 7. $\Delta = (\Delta v/v_0)_\omega - (\Delta v/v_0)_{30\,\mathrm{MHz}}$ for MnF_2 [001], 90-MHz data shifted upward 2×10^{-4}, 110-MHz shifted upward 14×10^{-4}.

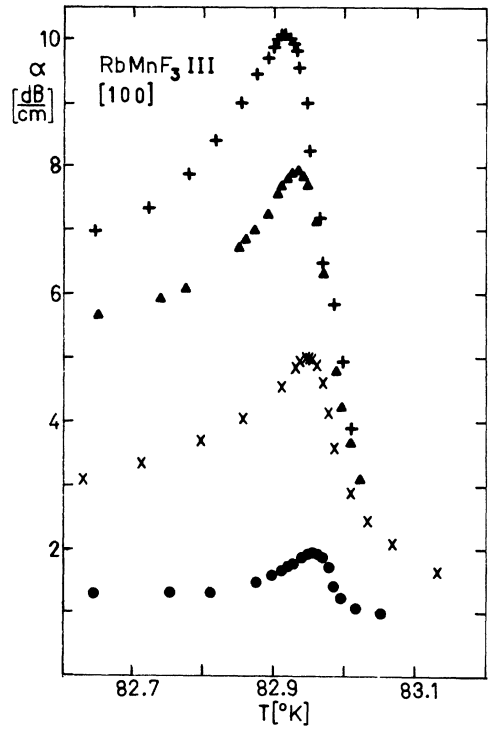

FIG. 8. Critical attenuation maxima for various frequencies near T_N for $RbMnF_3$ III[100]. ●, 90 MHz; ×, 150 MHz; ▲, 275 MHz; +, 390 MHz. Ordinate shifted.

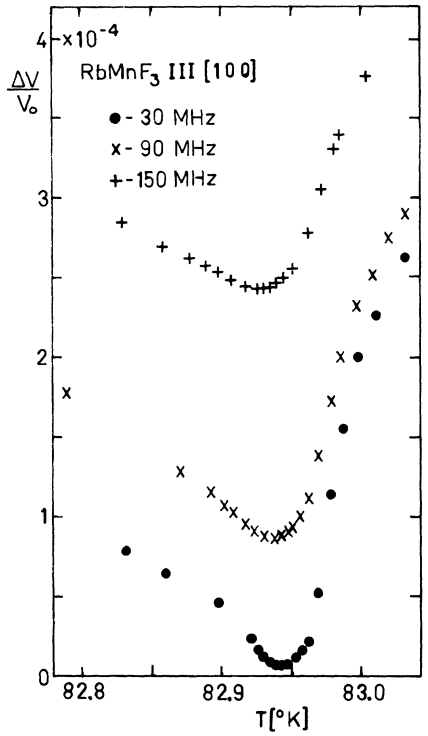

FIG. 9. Critical velocity minima for various frequencies near T_N for $RbMnF_3$ III [100].

observes a typical velocity minimum (which is shifted, however, about 15 mdeg at 30 MHz from the attenuation maxima which is taken to be T_N, as discussed in Sec. IV D), this is largely suppressed for the higher frequencies. In fact, at 90 and 110 MHz there is a small, but noticeable, maximum just at T_N. In the framework of a single relaxation-time theory (3b), this maximum can only be explained by a divergence of τ at T_N. We can make a quantitative comparison with (3b) by subtracting $(\Delta v/v)_\omega$ from $(\Delta v/v)_{30\,\mathrm{MHz}}$ to obtain the dispersion. The result near T_N is shown in Fig. 7. The maxima for all frequencies occur within 30 mdeg of T_N. The τ can be obtained from the ratio of the difference from 30 MHz for two higher frequencies and (3b). It is necessary to use a ratio since the 30-MHz velocity is also suppressed from the low-frequency critical change. The τ was found to remain approximately constant at $(2.7\pm0.2)\times10^{-9}$ sec down to $\epsilon = 10^{-3}$, in very good agreement with the value quoted in Ref. 8, and showed a slight divergence for smaller ϵ. At the smallest ϵ $(=1.5\times10^{-4})$ we measured $\tau = (4\pm0.2)\times10^{-9}$ sec. It should be noted that this temperature dependence of τ is much weaker than that found in $RbMnF_3$. The slight divergence of τ below $\epsilon = 10^{-3}$ could possibly be due to another relaxation mechanism becoming dominant, as was pointed out before in Ref. 8.

D. Sound Propagation in Ordered Region

In Figs. 8 and 9, we show attenuation and velocity changes in the vicinity of T_N for $RbMnF_3$ III. One clearly sees frequency-dependent shifts of the attenuation maxima and velocity minima. The velocity minima at each frequency occur ~ 20 mdeg lower than the corresponding attenuation maxima. Such a behavior has been observed before in MnTe,[19] in the rare-earth metals,[1] in Ni,[20] and in liquid He below T_λ.[21] A shift in attenuation maxima has been observed before in Ni[20] and in MnF_2.[9] In Table I, we list the temperature shifts of the attenuation maxima and velocity minima for the various $RbMnF_3$ crystals investigated with respect to the attenuation maximum for 70 MHz. From the frequency dependence of these temperature shifts one can conclude that the attenuation maximum for the lowest frequency measured (70 MHz) is at the Néel temperature within an accuracy of 5 mdeg. We used different extrapolation procedures, based on the values listed in Table I and shown in Figs. 8 and 9 (linear, semilog, and log-log plots) to extrapolate a T_N; all give the T_N listed in Table I within an accuracy of 5 mdeg for each crystal. All the experimental results discussed before for $T > T_N$ were evaluated with T_N determined in this way. It should be noted that a systematic error of up to 10 mdeg in this procedure would have a negligible effect on the evaluation and interpretation of our experiments in the paramagnetic region. The reason for this is partly the broadening of the transition for $\epsilon \lesssim 10^{-4}$ as discussed before (Sec. IV A and Ref. 7) and partly the fact that for higher frequencies the critical attenuation is less critically dependent on ϵ [see, e.g., Eq. (3a), Figs. 4 and 5, and Ref. 7].

Now we would like to discuss these temperature

TABLE I. Temperature shifts of critical attenuation maxima and velocity minima at various frequencies for samples of $RbMnF_3$. T_N chosen as attenuation maximum at 70 MHz.

Sample	I [111]	II [111]	III [100]
T_N (°K)	82.99 ± 0.01	82.93 ± 0.01	82.95 ± 0.01
Frequency (MHz)	Attenuation-peak shift (mdeg)		
90	2 ± 5	2 ± 5	2 ± 5
150	7 ± 5	7 ± 5	
270	16 ± 5	17 ± 5	22 ± 5
336	25 ± 5	40 ± 5	
395		49 ± 5	42 ± 5
	Velocity-minimum shift (mdeg)		
30	13 ± 4		14 ± 4
90	20 ± 4	15 ± 5	20 ± 5
150	34 ± 4	30 ± 5	27 ± 5

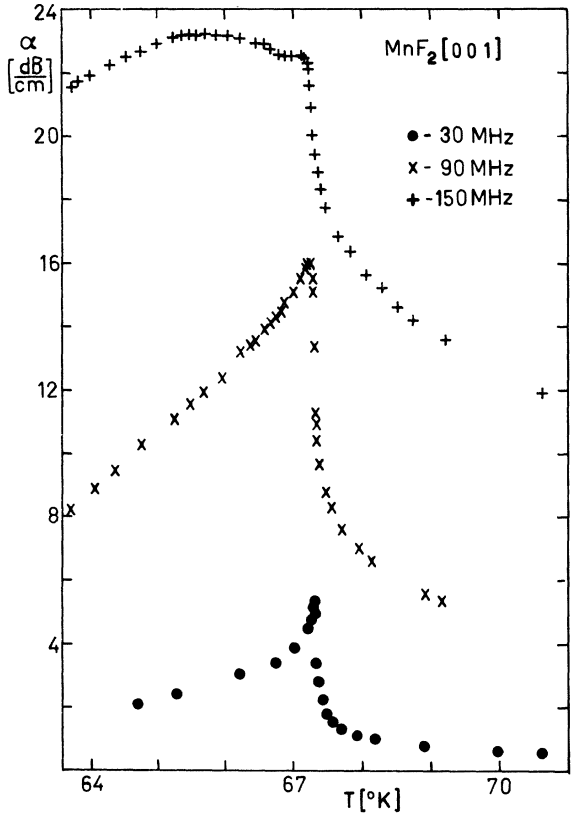

FIG. 10. Attenuation maxima for various frequencies in MnF_2.

shifts for $RbMnF_3$ and MnF_2 together with the additional attenuation peaks observed at lower temperatures. In Fig. 10, we show attenuation measurements for MnF_2 in the frequency range 30–150 MHz. For the highest frequency one clearly observes a broad maximum below T_N. From Ref. 9 it can be seen that at higher frequencies up to 955 MHz this peak shifts to lower temperatures with increasing frequency and the critical peak at T_N is masked. In $RbMnF_3$ one observes a distinct second peak below T_N at frequencies higher than 100 MHz as already shown in Fig. 1 and more completely for the three samples in Figs. 11 and 12. The results from these figures indicate that, while the attenuation peak at T_N is the same for all the samples, even the small temperature shifts according to Table I, this is not the case for the second attenuation peak in the ordered region. In fact, for a given frequency the strength of this peak as well as the temperature location is sample dependent. However, in all samples this subsidiary peak shifts to lower temperatures with increasing frequency. There are various possible reasons for this attenuation peak below T_N, such as domain effects, coupling of the sound wave to spin-wave modes, nuclear-acoustic resonance, or coupling to the order parameter. We shall discuss briefly these various possibilities.

1. *Domain Effects*

Very little is known about domain wall-stress effects in antiferromagnets. In ferromagnetic EuO, large sound-wave attenuation effects due to domains have been reported.[4,22] In ferromagnetic Ni magnetic hysteresis effects have been observed as close as $\epsilon \sim 10^{-4}$ to T_c.[23] In MnF_2, for longitudinal sound propagation along the c axis there is no stress-domain wall coupling since the easy axis is also along the c axis. In $RbMnF_3$, the easy axes are along the various [111] directions. The actual domain configuration will be determined by imperfections and local strains.[24] There is, therefore, a stress-domain wall interaction possible in this case.

2. *Coupling to Spin-Wave Modes*

There is the possibility that a resonant interaction between sound waves and spin waves gives additional attenuation and velocity changes in the ordered region. The reason for this is the fact that the spin-wave energy gap, which, for example, for a uniaxial antiferromagnet is given as $\omega_m(0) = \gamma(2H_{ex}H_a)^{1/2}$, is a rapidly varying function of temperature near T_N, because both the exchange field H_{ex} and anisotropy field H_a change rapidly with T. Therefore, there is the possibility of a crossover

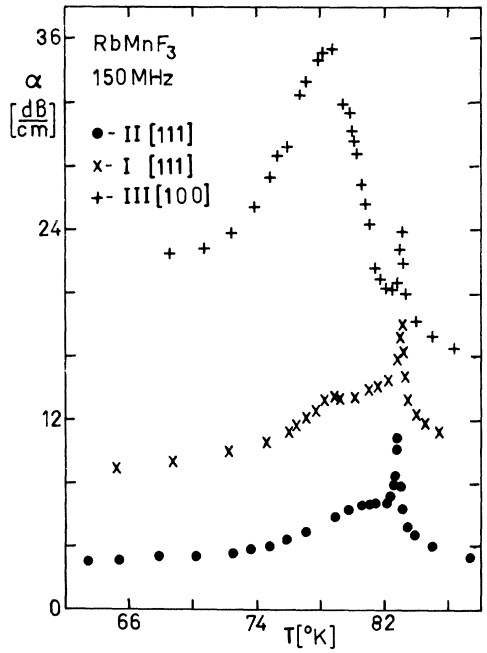

FIG. 11. Ordered-region attenuation peaks in $RbMnF_3$ at 150 MHz for three samples. Ordinate shifted to separate curves.

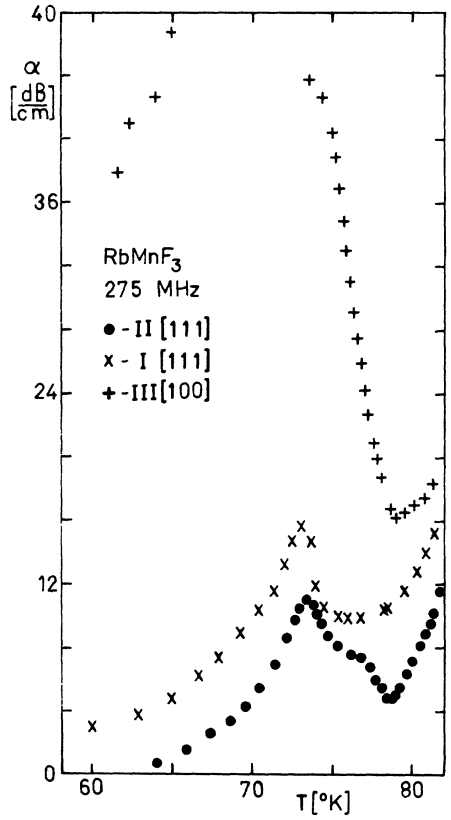

FIG. 12. Ordered-region attenuation peaks in $RbMnF_3$ at 275 MHz for three samples. Critical peak about 25 dB/cm at this frequency. Ordinate shifted to separate curves.

of the sound-wave and spin-wave dispersion spectra. Such effects are well known for ferrimagnets.[25] For the c_{33} mode in MnF_2, there is no linear magnetoelastic coupling to the magnetic modes[26] and, therefore, this process has to be ruled out in this case. For $RbMnF_3$, this coupling is possible[27]; however, in MnF_2 recourse to higher-order processes (sound-wave–spin-wave scattering) has to be made.

3. *Nuclear-Acoustic Resonance*

Additional frequency-dependent attenuation peaks in the ordered region of MnTe have been observed which are similar to the ones reported here and tentatively ascribed to a nuclear resonance absorption of the Mn^{55} nuclei.[19] Such an absorption due to the Mn^{55} nuclei has also been reported for $RbMnF_3$ at low temperatures and ~ 600 MHz.[28] This nuclear resonance absorption can, in principle, be operative both for MnF_2 and $RbMnF_3$.

The nature of these additional attenuation peaks shown in Figs. 11 and 12 will be studied further experimentally.[29] Whatever the nature of these peaks, they can, in principle, influence the location of the critical peak at T_N. Since we are talking of temperature shifts of some 50 mdeg for our frequency range (see Table I), a small tail of the attenuation peak in the ordered region could easily explain the shift of the critical peak in $RbMnF_3$. No definite conclusion can be reached, however, because of the smallness of the effect and the sample dependence of these additional peaks.

4. *Coupling to Order Parameter and Fluctuations*

So far we have not discussed yet the mechanism which gives rise to the pronounced singularities in the paramagnetic region. This process, namely, a sound-wave coupling either to spin fluctuations or spin energy density, should also be operative in the ordered region. Although no theory for $T < T_N$ has been worked out yet, it is conceivable that the attenuation behaves the same way as for $T > T_N$.[30] This means that, in order to study the temperature shifts quantitatively, one has first to subtract this effect. In addition there is, however, another mechanism which couples directly to the order parameter.[31] This process is thought to be responsible for the analogous effects observed at T_λ in He.[21] It leads to frequency-dependent attenuation maxima and velocity minima as observed in our case both for $RbMnF_3$ and MnF_2.

From the various possible origins of the additional attenuation peaks in the ordered region and the temperature shift of the critical peak at T_N, we can safely exclude the domain wall-stress effect and the resonant spin-wave–sound-wave absorption in the case of MnF_2. The nuclear-acoustic resonance attenuation is a possible explanation of the subsidiary attenuation peaks, although the sample-dependent attenuation curves of Figs. 11 and 12 indicate additional mechanisms in the case of $RbMnF_3$. It should be noted that while the critical attenuation temperature shifts are rather sample independent in $RbMnF_3$, as seen from Table I, this is not the case for the subsidiary attenuation peaks in the ordered region. Therefore the Landau-Khalatnikov mechanism, mentioned above, could still be the explanation for these critical temperature shifts. One has to wait for further theoretical and experimental development to interpret these results quantitatively.

V. CONCLUSION

In this paper we have shown that the sound propagation experiments in the paramagnetic region of $RbMnF_3$ and MnF_2 can be explained very well for both $\omega\tau < 1$ and $\omega\tau \gtrsim 1$ by assuming that the sound couples predominantly to the spin energy density rather than the spin fluctuations and that the spin-energy-density fluctuations, in turn, decay via spin-lattice relaxation. In fact the attenuation in $RbMnF_3$ is well described by a single relaxation-

time type of expression as shown in Eqs. (3). Likewise for $\omega\tau \gtrsim 1$ there is noticeable dispersion described by the frequency-dependent velocity given in Eq. (3b) and observed both for $RbMnF_3$ and MnF_2. Together with the result in EuO,[4,6,7] it is safe to say that for insulators, in general, the sound wave couples predominantly to the spin energy density. One expects then, in general, that the critical exponent η in insulators will always be much smaller than the one in magnetic metals. Until now, no exception to this rule has been found. To characterize sound-propagation effects in insulators one has to investigate the following properties: (a) spin-phonon coupling constant (whether it is of single-ion type or due to strain modulation of the exchange interaction); (b) range of the exchange forces. If the exchange force is mainly limited to nearest neighbors, then it is safe to assume that sound-wave–spin-energy-density coupling is predominant. In other cases contributions from sound-wave–spin-fluctuation coupling could be noticeable. (c) The extent to which zone-boundary phonons of the acoustic branch contribute to the spin-lattice relaxation is important as shown by the different magnitudes of τ_L in $RbMnF_3$, MnF_2, and EuO.[6]

There is still a theoretical problem left with regard to the sound-wave–spin-energy-density coupling. As pointed out before,[1,8] for certain propagation directions, only part of the spins couple to the sound wave. Therefore, the relaxation of only part of the spin energy density plays a role. Judging from our experimental results, it seems that this effect has no noticeable influence.

We also would like to comment on the velocity changes observed in EuO.[1,4] Since for the frequencies measured[1,4,6,7] $\omega\tau > 1$, the dispersive effects described by Eqs. (3) should be clearly noticeable. Indeed, the net critical velocity change obtained experimentally (Figs. 2 and 3 in Ref. 4) is much smaller than the one observed, for example, in $RbMnF_3$ (see Fig. 3), although the coupling constant for EuO is larger than for $RbMnF_3$. This clearly indicates a noticeable suppression of critical velocity changes. Since thermal-expansion corrections and the background choice are very important in this case, we cannot make any quantitative statements.

Kawasaki[10] has calculated the interesting case of high-frequency sound propagation in cases where the sound also couples to the spin fluctuations, i.e., where one has a whole spectrum of relaxation times and where the simple single relaxation-time formulas [Eqs. (3)] no longer hold. The rare-earth metals are good candidates to observe these effects,[1] especially Gd for which $\omega\tau_c \sim 1$ for $\nu = 300$ MHz at $\epsilon \sim 3\times10^{-3}$. Work on these aspects is in progress in our laboratory.

Turning to the ordered region, the main features observed here are the frequency-dependent shifts of attenuation maxima and velocity minima. In addition, new strong attenuation peaks were found in $RbMnF_3$ a few degrees below T_N. For $RbMnF_3$, this additional attenuation, whose cause is not clearly known, is possibly responsible for the aforementioned critical temperature shifts. A study of magnetic field dependence of these additional attenuation peaks might shed some light on its nature. In the case of MnF_2 it is possible that the single attenuation peak which lies below T_N is a greatly enhanced version of the subsidiary peak in $RbMnF_3$ and the critical peak is masked by this second peak.

ACKNOWLEDGMENTS

It is a pleasure to acknowledge discussions with Professor E. Abrahams, Professor R. A. Ferrell, Professor D. L. Huber, Professor K. Kawasaki, and Professor M. J. Stephen. Professor D. L. Huber and Professor K. Kawasaki were kind enough to send us preprints of their work.

---

*Work supported by National Science Foundation.

[1]For a recent review of sound propagation near magnetic phase transitions with a complete list of references, see B. Lüthi, T. J. Moran, and R. J. Pollina, J. Phys. Chem. Solids 31, 1741 (1970).

[2]K. Kawasaki, Phys. Letters 26A, 543 (1968).

[3]G. E. Laramore and L. P. Kadanoff, Phys. Rev. 187, 619 (1969).

[4]B. Lüthi and R. J. Pollina, Phys. Rev. Letters 22, 717 (1969).

[5]K. Kawasaki, Phys. Letters 29A, 406 (1969).

[6]D. L. Huber, Phys. Rev. B 3, 836 (1971).

[7]G. Gorodetsky, B. Lüthi, and T. J. Moran, in *Proceedings of the Fordham Conference on the Dynamical Aspects of Critical Phenomena, New York*, 1970, edited by J. I. Budnick and M. P. Kawatra (Gordon and Breach, New York, to be published).

[8]K. Kawasaki and A. Ikushima, Phys. Rev. B 1, 3143 (1970); A. Ikushima, J. Phys. Chem. Solids 31, 283 (1970); 31, 939 (1970).

[9]A. Bachellerie, Solid State Commun. 8, 1059 (1970).

[10]K. Kawasaki, in Ref. 7; Intern. J. Magnetism 1, 171 (1971).

[11]H. S. Bennett, Phys. Rev. 185, 801 (1969).

[12]V. N. Kashcheev, Phys. Letters 25A, 71 (1967).

[13]T. J. Moran and B. Lüthi, Phys. Rev. 187, 710 (1969).

[14]R. G. Leisure and R. W. Moss, Phys. Rev. 188, 840 (1969).

[15]D. T. Teaney, V. L. Moruzzi, and B. E. Argyle, J. Appl. Phys. 37, 1122 (1966).

[16]R. L. Melcher, D. I. Bolef, and R. W. H. Stevenson, Solid State Commun. 5, 735 (1967).

[17]B. Golding, Phys. Rev. Letters 20, 5 (1968).

[18]H. Y. Lau, L. M. Corliss, A. Delapalme, J. M. Hastings, R. Nathans, and A. Tucciarone, J. Appl. Phys. 41, 1384 (1970).
[19]K. Walther, Solid State Commun. 5, 399 (1967).
[20]B. Golding and M. Barmatz, Phys. Rev. Letters 23, 223 (1969).
[21]M. Barmatz and I. Rudnick, Phys. Rev. 170, 224 (1968).
[22]Y. Shapira and T. B. Reed, J. Appl. Phys. 40, 1197 (1969).
[23]G. Pepperl, D. Krause, and K. Stierstadt, Phys. Letters 31A, 75 (1970).
[24]W. J. Ince and A. Platzker, Phys. Rev. 175, 650 (1968).
[25]See, for example, Ref. 13.
[26]R. L. Melcher, Phys. Rev. B 2, 733 (1970).
[27]R. L. Melcher and D. I. Bolef, Phys. Rev. 186, 491 (1969); 178, 864 (1969). In these papers the additional attenuation peaks for $T < T_N$ have not been observed because the measurements were performed at 30 MHz only.
[28]J. B. Merry and D. I. Bolef, Phys. Rev. Letters 23, 126 (1969).
[29]Similar attenuation peaks have been observed in the ordered region at so-called spin reorientation transitions [T. J. Moran and B. Lüthi, J. Phys. Chem. Solids 31, 1735 (1970); G. Gorodetsky and B. Lüthi, Phys. Rev. B 2, 3688 (1970)]. However, in this case the attenuation maxima occur at the same temperature for all frequencies. In addition, $RbMnF_3$ is believed to have the same easy axis [111] for $T < T_N$.
[30]Attenuation results for low frequencies in Gd and MnF_2 indicate that the critical exponent is somewhat smaller for $T < T_N$ than it is for $T > T_N$ (see Refs. 1 and 8).
[31]L. D. Landau and I. M. Khalatnikov, Dokl. Akad. Nauk USSR 96, 469 (1954).

PHYSICAL REVIEW B VOLUME 4, NUMBER 1 1 JULY 1971

Magnetic Circular Dichroism of Sharp Optical Transitions in Antiferromagnetic FeF_2†

Ming Y. Chen, F. L. Scarpace, M. W. Passow,* and W. M. Yen
Department of Physics, University of Wisconsin, Madison, Wisconsin 53706
(Received 18 January 1971)

Using magnetic circular dichroic (MCD) modulation techniques, we have reinvestigated the spectrum of antiferromagnetic FeF_2, concentrating on pure electronic transitions and their associated magnetic structure. We show in this paper that because vibronically induced bands do not exhibit circular dichroism, MCD spectra complement absorption spectra in aiding our understanding of magnetic effects. In particular, we present the results of studies of the magnetic field and temperature dependence of the MCD spectra in two absorption regions of FeF_2, i.e., the 21 500- and 25 900-cm^{-1} regions, and report the effective g factors of all excitations, simple and compounded, in these two regions. In the 21 500-cm^{-1} region we report the identification of a two-magnon sideband and its thermal and magnetic properties; in the other, we observe an additional purely electronic transition which is obscured by broad-band absorption and appears only through its MCD properties. Several observations are made on the additional information obtainable by consideration of the polarity of the MCD signal in antiferromagnets.

The spectra of antiferromagnetic insulators have been actively investigated in recent years and the major features of these spectra are generally understood.[1] In this paper, we wish to report measurements of the magnetic circular dichroism (MCD) properties of antiferromagnetic FeF_2 in order to emphasize that MCD can serve as a powerful complementary aid to our analysis of the absorption spectra in these materials. Hitherto, MCD and its associated Faraday rotation have been proved useful in the interpretation of the spectra of color centers, nonmagnetic insulators,[2] and ionic solutions.[3] The majority of the studies cited have involved broad-band spectra and only a few have utilized modulation techniques to detect small MCD signals.

In this paper, we present results of a high-resolution (~0.1 Å) study of the MCD of sharp optical transitions in the 21 000- and 25 800-cm^{-1} absorption bands of FeF_2. This type of a study is then shown to provide additional important information concerning the nature of excitations, the active light operator for the transitions, and their reaction to external perturbation. The MCD of the transitions, further, have allowed us to identify a previously unreported purely electronic magnetic-dipole transition in the 25 800-cm^{-1} band and an extremely weak two-magnon sideband in the 21 000-cm^{-1} region. MCD signals are observed for purely electronic magnetic-dipole (π-, α-active) transitions and one- and two-magnon sidebands, but none have been observed for vibronically induced bands in any of the antiferromagnets we have investigated to date. It is this simplification of the MCD signal over the complex absorption spectrum that underscores the usefulness